ACS APPLIED MATERIALS & INTERFACES

www.acsami.org

Research Article

Naringin@Metal–Organic Framework as a Multifunctional Bioplatform

Xueying Ge, Fangchao Jiang, Minghui Wang, Meng Chen, Yiming Li, Joshua Phipps, Jianfeng Cai, Jin Xie, Jane Ong, Viktor Dubovoy, James G. Masters, Long Pan,* and Shengqian Ma*

Cite This: *ACS Appl. Mater. Interfaces* 2023, 15, 677–683

Read Online

ACCESS | Metrics & More | Article Recommendations | Supporting Information

ABSTRACT: Naringin, a natural product, can be used as a therapeutic agent due to its low systemic toxicity and negligible adverse effect. However, due to its hydrophobic nature and thereby low solubility, high-dose treatment is required when used for human therapy. Herein, we demonstrate the employment of a metal–organic framework (MOF) as a nontoxic loading carrier to encapsulate naringin, and the afforded nairngin@MOF composite can serve as a multifunctional bioplatform capable of treating Gram-positive bacteria and certain cancers by slowly and progressively releasing the encapsulated naringin as well as improving and modulating immune system functions through synergy between naringin and the MOF.

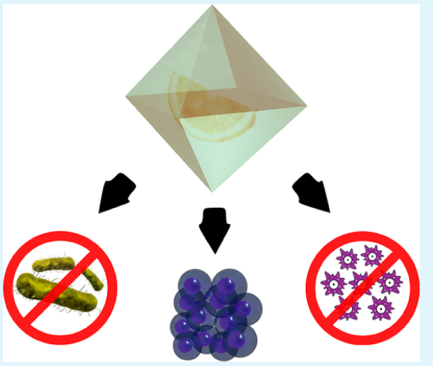

KEYWORDS: *cancer, Gram-positive bacteria, immune function, metal–organic framework, naringin*

1. INTRODUCTION

Natural products utilized as therapeutic agents as described in *The Grand Compendium of Materia Medica* have been recognized since the ancient time due to their chemical diversity and biochemical specificity.[1,2] Despite the recent rapid development of synthetic drugs, therapeutic agents derived from natural products still contribute extensively to medical treatments due to their inherent biocompatibility and negligible adverse effects.[3] It is worth noting that natural products can also be treated as adjuvants, which are capable of improving and modulating the immune system function.[4] Among these are flavonoids,[5,6] a bioactive group of the secondary metabolites found in various edible fruits, vegetables, and medicinal plants, which exhibit pharmacological activities as antioxidants[7] and anti-inflammatory drugs.[8] The flavonoid's phenolic moiety allows it to kill bacteria[9] and serve as an alternative food preservative. Naringin, a flavanone-glycoside compound that is the source of a bitter taste in grapefruit juice, has sparked a growing interest in treating various diseases due to its wide bioavailability, pharmacological versatility, and low cost.[10] However, the therapeutic efficacy of naringin is limited because of its poor solubility in aqueous media, susceptibility to pH, and ease of oxidation,[11] presenting a challenge for its use in further medical treatments. Thus, protecting its oxidation and improving its solubility in aqueous solutions via loading into nanocarriers could facilitate an increase in its therapeutic efficiency.

Considerable attention has recently been focused on hybrid porous solids known as metal–organic frameworks (MOFs), given their high surface areas, tunable structures, and controllable porosities, which have been explored for a wide variety of drug delivery applications.[12−15] By judiciously choosing the chemical compositions, sizes, structures, and surface properties, MOFs can be rendered with biocompatibility and biosafety.[12,16] Their amphiphilic internal microenvironment caused by the coordination interaction between the polar metal ions and the nonpolar organic ligands makes them well suited to encapsulate both hydrophilic and hydrophobic drugs.[16,17] Therefore, MOFs could be suitable carriers for loading naringin to increase its therapeutic efficiency and avoid the possibility of naringin aggregation upon intravenous administration.[18]

Enteric bacteria such as *Bacillus subtilis (B. subtilis)*, a Gram-positive bacterium, are the primary etiological agents of epidemic diarrhea and are sporadic in adults and children.[19] However, due to the deep decline in antibiotic approval over the last 30 years,[20] natural products discovered as antibiotics to treat such ailments have received enormous attention. Naringin is widely used to treat bacteria due to it containing a phenolic structure, which can disrupt the bacterial membrane

Received: November 5, 2022
Accepted: December 7, 2022
Published: December 23, 2022

Scheme 1. Illustration of Loading Naringin into MIL-101 as a Multifunctional Bioplatform with Antibacterial, Cancer Cell Killing, and Immune Cell Promoting Properties

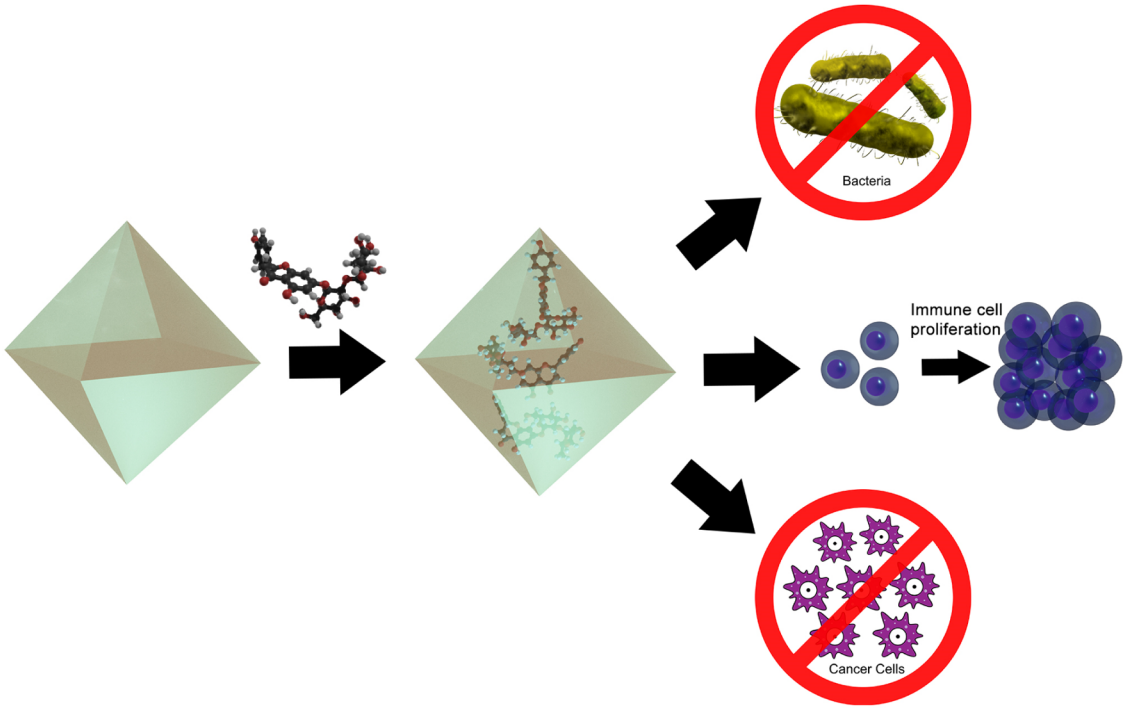

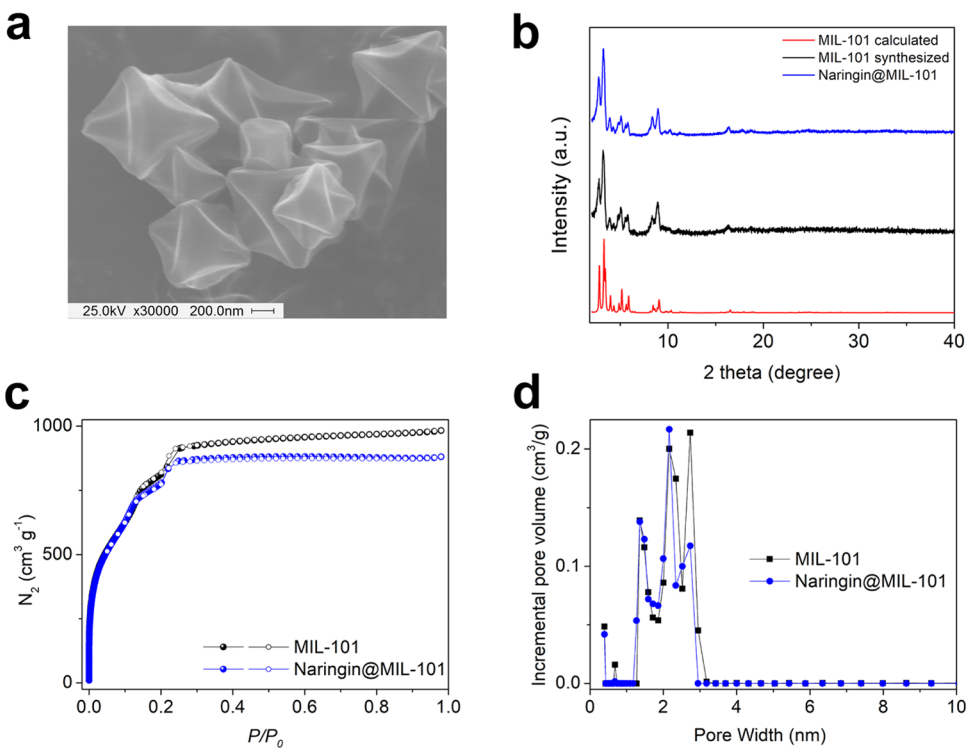

Figure 1. (a) Scanning electron microscopy image of MIL-101; (b) powder X-ray diffraction (PXRD) patterns of MIL-101 (black line) and naringin@MIL-101 (blue line); (c) N_2-sorption isotherms of MIL-101 (black line) and naringin@MIL-101 (blue line) (solid one: adsorption; empty one: desorption); and (d) pore size distribution curves of MIL-101 (black line) and naringin@MIL-101 (blue line).

structures, resulting in the leakage of cellular components and, thereby, cell death.[21] However, it is generally more active against Gram-negative than Gram-positive bacteria.[8] Therefore, using a carrier that can penetrate the Gram-positive bacteria peptidoglycan layer to release naringin for its treatment is critical. Alternatively, using MOFs as carriers to encapsulate naringin could solve this issue and increase the antibacterial effectiveness due to a coordination interaction within the peptidoglycan layer of Gram-positive microbes where lipoteichoic acid can serve as a chelating agent to

https://doi.org/10.1021/acsami.2c19904
ACS Appl. Mater. Interfaces 2023, 15, 677−683

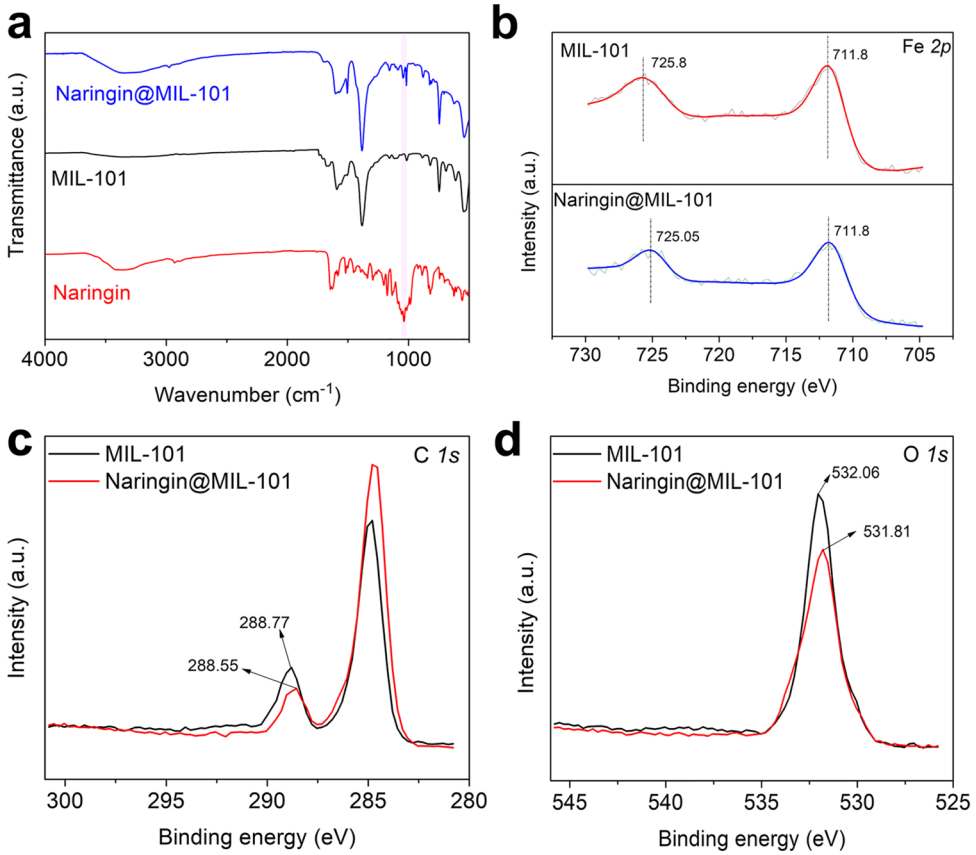

Figure 2. (a) Fourier transform infrared (FTIR) spectra of MIL-101 and naringin@MIL-101 compared with naringin; (b) Fe 2p, (c) C 1s, and (d) O 1s XPS spectra of MIL-101 and naringin@MIL-101.

coordinate with the metal ion in the MOF structure, thus possibly resulting in a membrane damage through lipid peroxidation, leading to the inactivation of Gram-positive microbes like *B. subtilis*.[22,23]

Bacteria, as an antigen, can trigger an immune response in an effort to defend themselves. As a natural antibiotic, naringin can confer protection against bacteria and be used as an immune adjuvant to modulate the immune system.[4,24] MOFs as naringin delivery vehicles could also be used as potential immune activators due to their intrinsic immunogenicity behavior.[25]

Recent epidemiological studies have shown that high dietary consumption of vegetables and fruits reduces the risks of certain types of cancer.[26] Therefore, the naringin-loaded MOF has the potential to establish natural product therapeutic modes for combinational therapy, providing antibacterial and antitumor treatment along with boosting the immune system. Multifunctional theranostic systems coordinated with individual functions can optimize therapeutic efficiency, therefore providing more opportunities for on-demand therapy, as well as paving the road toward precision medicine. To the best of our knowledge, the naringin-loaded MOF used for multifunctional treatment has not yet been reported.

In this work, a nontoxic iron (III)-based MOF, MIL-101(Fe) (denoted as MIL-101),[17] was chosen as the platform to load naringin due to its large loading capacity,[27] high porosity, biodegradability caused by the labile metal−ligand bonds, and its hydrophobic and hydrophilic properties. These attributes combine to make it an ideal candidate as a naringin delivery vehicle to achieve multifunctional therapy.[28] The structure of MIL-101[29,30] features two mesocages with two windows that are ideally sized to allow naringin to easily diffuse into the pores and reside within the mesocages. Moreover, the hydrophobic interaction between naringin and the MOF structure enables sustained release to reduce the total dose of naringin medication required. We speculate that the naringin-loaded MOF composite can synergize in killing *B. subtilis*, which can be measured by antibacterial activity. The viability of immune and cancer cells is also tested to further explore the naringin-loaded MOF as a promising target for multifunctional therapy (Scheme 1).

2. RESULTS AND DISCUSSION

MIL-101 was synthesized by a hydrothermal method and isolated by centrifugation. As shown in Figure 1a scanning electron microscopy image, as-synthesized MIL-101 nanoparticles have an octahedral shape with a side length of about 1 μm. According to Figure 1b, the powder X-ray diffraction (PXRD) pattern of synthesized MIL-101 matches well with the calculated one. Naringin@MIL-101 composites were prepared through a stepwise method: First, MIL-101 was activated under vacuum after immersing the as-synthesized samples in acetone to exchange the nonvolatile solvent (*N*,*N*-dimethylformamide (DMF)). Subsequently, the activated MIL-101 powder was added to the naringin solution as shown in Figure S2. After stirring the solution for 1 h, the final composite powder, naringin@MIL-101, was centrifuged and washed with the corresponding solution to remove the excess naringin on the exterior surface of MIL-101. Due to naringin's hydrophobic properties, various ratios of aqueous and ethanol solutions

https://doi.org/10.1021/acsami.2c19904
ACS Appl. Mater. Interfaces 2023, 15, 677−683

were used as loading solutions to dissolve naringin. The loading concentration of naringin was fixed to 1 mg mL^{-1}. The loading efficiency and capacity of naringin within MIL-101 were determined by ultraviolet−visible (UV−vis) spectroscopy.

The naringin@MIL-101 composite structure was digested by a 40% hydrofluoric acid aqueous solution. Subsequently, methanol was added to the acid solution to dissolve the sample since the ligand (terephthalic acid, denoted as BDC) is not soluble in methanol but naringin is. In this regard, the undissolved BDC ligand can be removed by the syringe filter. The content of naringin in methanol can be measured by UV−vis spectroscopy. When more water was introduced to the naringin-dissolved solution, more naringin was observed to be encapsulated into the MOF structure likely due to the hydrophobic interaction between naringin and the MIL-101 structure. As shown in Table S1, the mixed solution with a ratio of 1:2.2 (ethanol/water) used for naringin loading was found to be the optimal ratio since the loading capacity is the highest as compared to the others, which is ∼12 wt % (Figure S1 and Table S1). PXRD of MIL-101 immersing into the mixed solution was taken to show the integrity of the MOF structure (Figure S3), suggesting that the mixed solution did not cause any damage to the MOF structure.

Since the ratio of 1:2.2 (ethanol/water) is the optimal ratio to load naringin into MIL-101, the naringin@MIL-101 composites produced under this condition are the main research object for the below characterization and drug loading with their antibacterial, anticancer, and immune applications. To further characterize the structure of naringin@MIL-101 composites, PXRD patterns (Figure 1b) were measured to prove that it is consistent with those of the synthesized and calculated MIL-101, revealing that the MOF structure remained intact after loading naringin. Nitrogen sorption isotherms were collected at 77 K, and the Brunauer−Emmett−Teller surface area (S_{BET}) for naringin@MIL-101 was calculated to be 2927 m^2/g, showing a drop compared to the pristine MIL-101 with a surface area of 3124 m^2/g (Figure 1c) due to the naringin loading. As evident from pore size distribution, the pore volume was decreased from 1.51 to 1.39 cm^3/g, indicating that naringin occupied the pores, thereby reducing the pore volume and S_{BET} (Figure 1d). The TGA profile (Figure S4) of the naringin@MIL-101 composite suggested around 12 wt % loss compared with MIL-101 due to the presence of naringin, which is consistent with the loading percentage monitored by UV−vis. As shown in Table S2, there is an increase in carbon and hydrogen wt % of naringin@MIL-101 compared with MIL-101. Furthermore, an X-ray photoelectron spectroscopy (XPS) survey showed that Fe atomic % is decreased when naringin is loaded inside MIL-101 (Figure S5b), suggesting that naringin was loaded inside of the MOF structure.

The combination of naringin and MIL-101 was confirmed by Fourier transform infrared (FTIR) spectra. As shown in Figure 2a, a band around 1044 cm^{-1}, associated with the naringin C−O strong vibration, was observed in naringin@MIL-101 composites but not in MIL-101. Figure S5a showed that the C−O vibration spectra of naringin@MIL-101 was shifted to a higher wavenumber than naringin, indicating an interaction between naringin and MIL-101. X-ray photoelectron spectroscopy (XPS) spectra of MIL-101 and naringin@MIL-101 were used to verify the interaction between naringin and MIL-101 further. As shown in Figure 2b−d, the Fe $2p_{1/2}$ peak, C 1s peak, and O 1s peak of naringin@MIL-101 were shifted around 0.75 eV toward lower binding energy compared to MIL-101, indicating an electron transfer from MIL-101 to naringin. This shows that the MOF, as an electron donor, provides more electrons to naringin, which may be the leading cause of the naringin@MIL-101 composites' synergistic antibacterial effect.

Figure 3 displays a time-course measurement of naringin delivery to an aqueous solution in a dialysis bag at room

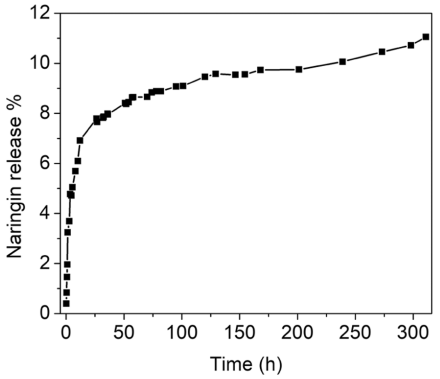

Figure 3. *In vitro* naringin release profile from naringin@MIL-101.

temperature with continuous stirring. The released amount of naringin was quantified via UV−vis spectroscopy by taking out the released solution at a certain time interval. Only 7.8 wt % of naringin was released after 26 h. The sustained release was observed with only 11 wt % of naringin releasing after 13 days. This slow release satisfies the daily need for naringin uptake to avoid multidose side effects. The release of naringin from naringin@MIL-101 composites was analyzed by the mathematical models of Sahlin−Peppas, Ritger−Peppas, and Higuchi equations described in the Supporting Information.[31] The nonlinear fitted curves with three models are shown in Figure S6. The correlation coefficient (R^2) and the fitting parameters, as shown in Table 1, were used to determine the fit's quality

Table 1. Result of Fitting the Drug Release Model

kinetic model	R^2	k_1	k_2	m	n
Sahlin−Peppas	0.967	3.08	−0.23	0.34	
Ritger−Peppas	0.923	3.45			0.21
Higuchi	0.237	0.85			

and predict the drug release profile. These results indicate that the released mathematical model of the drug from naringin@MIL-101 composites was fit for the Sahlin−Peppas model, which is controlled by the combination of Fickian diffusion and Case-II relaxation. Fickian diffusion is controlled by the concentration difference. Even though the MOF is biodegradable, its structure is robust. Thus, Case-II relaxation would happen in this situation since the drug diffusion is rapid compared to the relaxation of MOF carriers.[32]

The antibacterial activity of naringin@MIL-101 was tested against *B. subtilis*, a Gram-positive bacterium, as shown in Table 2. Minimal inhibitory concentrations (MICs) were determined by the microdilution method using clinical strains of *B. subtilis*. Naringin@MIL-101 showed a significantly decreased MIC value (0.93 ± 0.33 mg/mL) as compared to pure naringin (5 mg/mL) and MIL-101 (1.88 ± 0.62 mg/mL).

https://doi.org/10.1021/acsami.2c19904
ACS Appl. Mater. Interfaces 2023, 15, 677−683

Table 2. Antibacterial Activities of Naringin@MIL-101 Compared with Naringin and MIL-101 against *B. subtilis*

material	minimum inhibitory concentration value [mg/mL]
MIL-101	1.88 ± 0.62
naringin	5
naringin@MIL-101	0.93 ± 0.33

The dyes 4′,6-diamidino-2-phenylindole (DAPI, blue fluorescence) and propidium iodide (PI, red fluorescence) were applied to stain *B. subtilis* to conduct a fluorescence microscopy assay. Only blue fluorescence was observed when *B. subtilis was* not treated with naringin@MIL-101 composites. By contrast, blue and red fluorescences were both observed when the bacteria strains were treated with naringin@MIL-101 composites, indicating that the naringin@MIL-101 composites have an antibacterial effect (Figure 4). The high MIC value of naringin is required to kill Gram-positive bacteria[8] compared to the other two samples (Table 2) because of naringin's acidic properties, which make it more difficult to penetrate *B. subtilis* peptidoglycan layer. Even though hydroxyl groups are present in the naringin structure, they still do not promote the level of antibacterial effectiveness needed for the treatment of Gram-positive bacteria.[8] In this regard, MIL-101 increased the chance of killing *B. subtilis* since lipoteichoic acid in the peptidoglycan layer of Gram-positive microbes could serve as a chelating agent to coordinate with the metal ion in the MIL-101 structure, thus resulting in membrane damage through lipid peroxidation to inactivate Gram-positive microbes.[22] Furthermore, the flavonoid group in naringin could promote bacterial death after membrane damage along with naringin release. This coordination effect, in conjunction with the delivery of the flavonoid containing naringin via MIL-101 has the capability to offer a two-pronged attack promoting *B. subtilis* death.

As shown in the XPS data in Figure 2b–d, it is observed that MIL-101 transferred electrons to naringin, which may account for naringin@MIL-101 composites killing more *B. subtilis*. It is also confirmed by the band gap monitored by solid UV–vis, as shown in Figure S7. This band gap of naringin@MIL-101 was 2.68 eV, showing a decrease compared with pure naringin (3.17 eV), which suggested that MIL-101 transferred electrons to naringin. This finding indicates that high kinetic activity impedes free radicals' scavenging, thus improving the composite's antioxidant properties,[33] which is a potential mechanism for killing cancer cells. The evidence is provided in the results below. As shown in Figure 5a, the cell viability of H1299 mouse lung cells treated with naringin@MIL-101 was decreased compared with naringin and MIL-101, demonstrating naringin loading into MIL-101 can increase the chance of killing cancer cells.

To explore the immune function of naringin@MIL-101, naringin and naringin@MIL-101 were used to treat EL4 T cells (Figure 5b). The viability study revealed higher cell viability for the naringin@MIL-101 group than for the naringin-only group. Also, we did not see significant viability drops at the concentration range of 0–200 μg/mL, indicating naringin@MIL-101 composites are relatively safe for immune cells. To evaluate the immune cells' activation, the released cytokines from EL4 T cells were investigated via coincubation. Briefly, EL4 T cells were treated with three materials (naringin, MIL-101 and naringin@MIL-101) for 24 h. After that, the upper supernatants were extracted, and enzyme-linked immunosobent assay (ELISA) kits were used to test the activities of interleukin-2 (IL-2) and tumor necrosis factor-α (TNFα). As shown in Figure 5c, TNFα, a proinflammatory growth factor, has a lower activity for naringin@MIL-101 compared with naringin and MIL-101. In contrast, IL-2, an anti-inflammatory T-cell growth factor, has the highest activity for naringin@MIL-101 compared to the MIL-101 and naringin. It is worth mentioning that IL-2 produced by EL4 cells can activate the function of several immune cells such as natural killer cells and helper T-cells. This implies that naringin@MIL-101 could promote the IL-2 activity, thus stimulating proliferation and enhancing the function of T cells. Therefore, naringin@MIL-101 could affect the activation of the immune system. As primary effector cells of the innate immune response, T cells, a type of natural killer cell, possess the function of eliminating pathogens.[34] Thus, naringin@MIL-101 could affect T-cell proliferation by promoting the anti-inflammatory effect and inhibiting the inflammatory response. We believe by further increasing the incubation time, cell confluency, or material concentrations, we can readily promote cytokine releases from naringin@MIL-101 composites, thereby inducing an increase in the immune response against EL4 T cells.

3. CONCLUSIONS

In summary, we show that naringin can be successfully loaded into the mesocage of MIL-101 in a short period of time

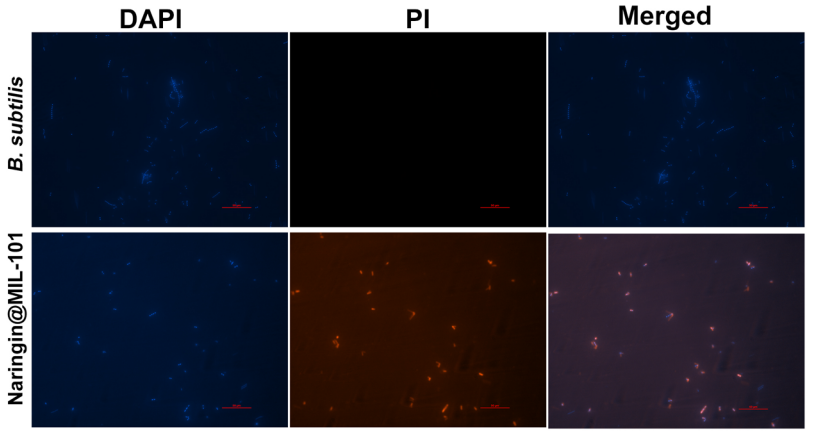

Figure 4. Confocal fluorescence images of *B. subtilis* treated with naringin@MIL-101 at two times MICs. The scale bar indicates a length of 50 μm.

https://doi.org/10.1021/acsami.2c19904
ACS Appl. Mater. Interfaces 2023, 15, 677–683

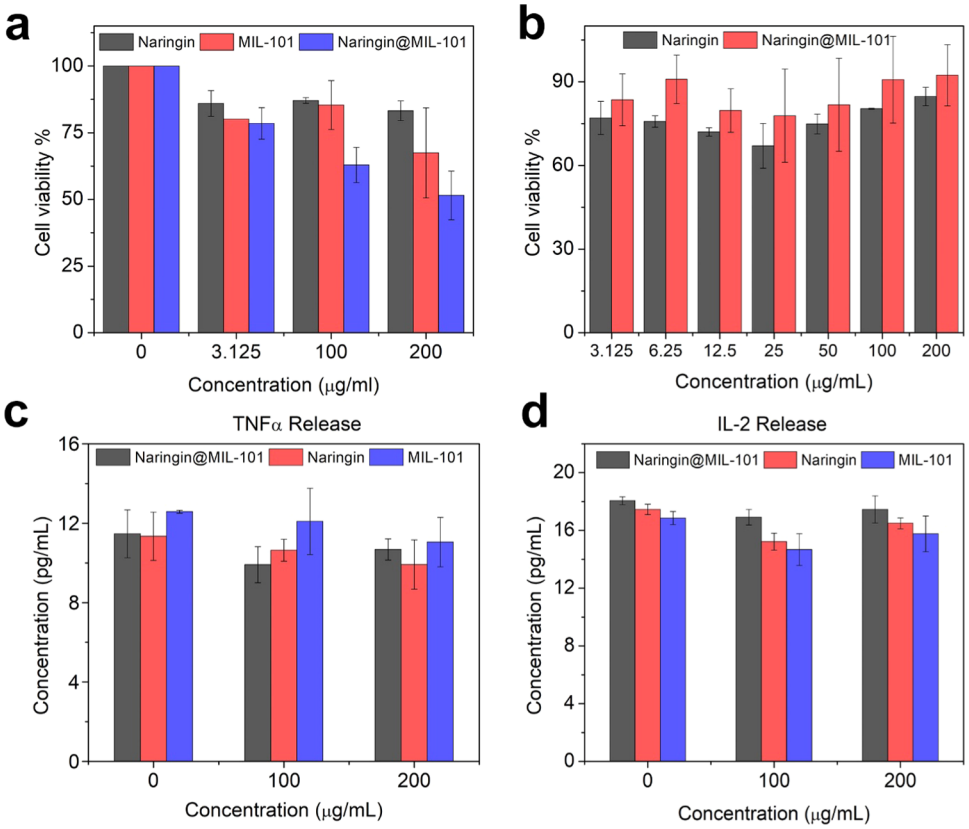

Figure 5. (a) H1299 cell cytotoxicity treated with naringin, MIL-101, and naringin@MIL-101; (b) EL4 T-cell viability treated with naringin and naringin@MIL-101; (c) TNFα and (d) IL-2 activities in EL4 T cells treated with naringin, MIL-101, and naringin@MIL-101.

through hydrophobic interactions. The composite, naringin@MIL-101, is capable of slow release, which lends itself to substantially reducing the chance of high dosage and side effects including minimal luminal naringin accumulation and symmetric arterial naringin deposition.[35] Naringin@MIL-101 composites show a better antibacterial effect toward Gram-positive bacteria than MIL-101 and naringin due to the coordination interaction between the MOF structure and the bacterial peptidoglycan layer, resulting in the death of the bacteria. Moreover, naringin@MIL-101 composites promote the growth of T cells by stimulating the proliferation of the IL-2 growth factor and can also be used to kill cancer cells. These antibacterial, anticancer, and immune-boosting properties make naringin@MIL-101 an excellent multifunctional bioplatform to achieve multitherapeutic effects.

■ ASSOCIATED CONTENT

Supporting Information

The Supporting Information is available free of charge at https://pubs.acs.org/doi/10.1021/acsami.2c19904.

UV−vis absorbance of naringin; pictures of loading solution; PXRD of MIL-101; TGA profile, elemental analysis, amplified IR, and XPS of MIL-101 and naringin@MIL-101; nonlinear naringin release curve fit and Tauc plot for naringin and naringin@MIL-101 (PDF)

■ AUTHOR INFORMATION

Corresponding Authors

Long Pan − *Colgate Palmolive Co, Piscataway, New Jersey 08855, United States;* orcid.org/0000-0003-0438-4040; Email: long_pan@colpal.com

Shengqian Ma − *Department of Chemistry, University of North Texas, Denton, Texas 76201, United States;* orcid.org/0000-0002-1897-7069; Email: Shengqian.Ma@unt.edu

Authors

Xueying Ge − *Department of Chemistry, University of North Texas, Denton, Texas 76201, United States*

Fangchao Jiang − *Department of Chemistry, University of Georgia, Athens, Georgia 30602, United States*

Minghui Wang − *Department of Chemistry, University of South Florida, Tampa, Florida 33620, United States*

Meng Chen − *Department of Chemistry, University of South Florida, Tampa, Florida 33620, United States*

Yiming Li − *Department of Chemistry, University of South Florida, Tampa, Florida 33620, United States*

Joshua Phipps − *Department of Chemistry, University of North Texas, Denton, Texas 76201, United States*

Jianfeng Cai − *Department of Chemistry, University of South Florida, Tampa, Florida 33620, United States;* orcid.org/0000-0003-3106-3306

Jin Xie − *Department of Chemistry, University of Georgia, Athens, Georgia 30602, United States;* orcid.org/0000-0002-8915-6233

Jane Ong − *Colgate Palmolive Co, Piscataway, New Jersey 08855, United States*

https://doi.org/10.1021/acsami.2c19904
ACS Appl. Mater. Interfaces 2023, 15, 677−683

Viktor Dubovoy − *Colgate Palmolive Co, Piscataway, New Jersey 08855, United States*
James G. Masters − *Colgate Palmolive Co, Piscataway, New Jersey 08855, United States*

Complete contact information is available at: https://pubs.acs.org/10.1021/acsami.2c19904

Notes

The authors declare no competing financial interest.

■ ACKNOWLEDGMENTS

The authors acknowledge the Robert A. Welch Foundation (B-0027) for financial support of this work.

■ REFERENCES

(1) Li, M.; Liang, Y. Li Shizhen and The Grand Compendium of Materia Medica. *J. Tradit. Chin. Med. Sci.* **2015**, *2*, 215−216.
(2) Koehn, F. E.; Carter, G. T. The Evolving Role of Natural Products in Drug Discovery. *Nat. Rev. Drug Discovery* **2005**, *4*, 206−220.
(3) Amedei, A.; D'Elios, M. M. New Therapeutic Approaches by Using Microorganism-Derived Compounds. *Curr. Med. Chem.* **2012**, *19*, 3822−3840.
(4) Jiang, L.; Zhang, G.; Li, Y.; Shi, G.; Li, M. Potential Application of Plant-Based Functional Foods in the Development of Immune Boosters. *Front. Pharmacol.* **2021**, *12*, No. 637782.
(5) Rucker, R. B. Flavonoids. In *Flavonoids in Health and Disease*; Rice-Evans, C. A.; Packer, L., Eds.; Marcel Dekker, Inc.: New York, 2004; Vol. *79*, pp 891−892.
(6) Cody, V.; Middleton, E.; Harborne, J. B.; Beretz, A. *Plant Flavonoids in Biology and Medicine II: Biochemical, Cellular, and Medicinal Properties*; Liss: New York, 1989; Vol. *280*.
(7) Pietta, P.-G. Flavonoids as Antioxidants. *J. Nat. Prod.* **2000**, *63*, 1035−1042.
(8) Adamczak, A.; Ozarowski, M.; Karpiński, T. M. Antibacterial Activity of Some Flavonoids and Organic Acids Widely Distributed in Plants. *J. Clin. Med.* **2020**, *9*, 109.
(9) Gyawali, R.; Ibrahim, S. A. Natural Products as Antimicrobial Agents. *Food Control* **2014**, *46*, 412−429.
(10) Chen, R.; Qi, Q. L.; Wang, M. T.; Li, Q. Y. Therapeutic Potential of Naringin: an Overview. *Pharm. Biol.* **2016**, *54*, 3203−3210.
(11) Rao, K.; Imran, M.; Jabri, T.; Ali, I.; Perveen, S.; Shafiullah; Ahmed, S.; Shah, M. R. Gum Tragacanth Stabilized Green Gold Nanoparticles as Cargos for Naringin Loading: a Morphological Investigation through AFM. *Carbohydr. Polym.* **2017**, *174*, 243−252.
(12) Rojas, S.; Arenas-Vivo, A.; Horcajada, P. Metal-Organic Frameworks: a Novel Platform for Combined Advanced Therapies. *Coord. Chem. Rev.* **2019**, *388*, 202−226.
(13) Cai, W.; Chu, C. C.; Liu, G.; Wáng, Y. X. Metal-Organic Framework-Based Nanomedicine Platforms for Drug Delivery and Molecular Imaging. *Small* **2015**, *11*, 4806−4822.
(14) Yang, J.; Yang, Y.-W. Metal—Organic Frameworks for Biomedical Applications. *Small* **2020**, *16*, No. 1906846.
(15) Ge, X.; Wong, R.; Anisa, A.; Ma, S. Recent Development of Metal-Organic Framework Nanocomposites for Biomedical Applications. *Biomaterials* **2022**, *281*, No. 121322.
(16) Rojas, S.; Colinet, I.; Cunha, D.; Hidalgo, T.; Salles, F.; Serre, C.; Guillou, N.; Horcajada, P. Toward Understanding Drug Incorporation and Delivery from Biocompatible Metal-Organic Frameworks in View of Cutaneous Administration. *ACS Omega* **2018**, *3*, 2994−3003.
(17) Horcajada, P.; Chalati, T.; Serre, C.; Gillet, B.; Sebrie, C.; Baati, T.; Eubank, J. F.; Heurtaux, D.; Clayette, P.; Kreuz, C.; Chang, J. S.; Hwang, Y. K.; Marsaud, V.; Bories, P. N.; Cynober, L.; Gil, S.; Ferey, G.; Couvreur, P.; Gref, R. Porous Metal-Organic-Framework Nanoscale Carriers as a Potential Platform for Drug Delivery and Imaging. *Nat. Mater.* **2010**, *9*, 172−178.
(18) Sun, T.; Zhang, Y. S.; Pang, B.; Hyun, D. C.; Yang, M.; Xia, Y. Engineered Nanoparticles for Drug Delivery in Cancer Therapy. *Angew. Chem., Int. Ed.* **2014**, *53*, 12320−12364.
(19) Grace, E. S. C.; Annamalai, A.; Ponmari, G.; Vani, C.; Rose, A.; Marahatta, A. B.; Gunasekaran, V. Cytotoxicity and Antibacterial Characteristics of Graphene-Oxide Nanosheets Toward Human Pathogens. *J. Nanosci. Nanotechnol.* **2016**, *16*, 2447−2452.
(20) Ryan, E. J.; Ryan, A. J.; Gonzalez-Vazquez, A.; Philippart, A.; Ciraldo, F. E.; Hobbs, C.; Nicolosi, V.; Boccaccini, A. R.; Kearney, C. J.; O'Brien, F. J. Collagen Scaffolds Functionalised with Copper-Eluting Bioactive Glass Reduce Infection and Enhance Osteogenesis and Angiogenesis Both in Vitro and in Vivo. *Biomaterials* **2019**, *197*, 405−416.
(21) Bouarab Chibane, L.; Degraeve, P.; Ferhout, H.; Bouajila, J.; Oulahal, N. Plant Antimicrobial Polyphenols as Potential Natural Food Preservatives. *J. Sci. Food Agric.* **2019**, *99*, 1457−1474.
(22) Zhuang, W.; Yuan, D.; Li, J. R.; Luo, Z.; Zhou, H. C.; Bashir, S.; Liu, J. Highly Potent Bactericidal Activity of Porous Metal-Organic Frameworks. *Adv. Healthcare Mater.* **2012**, *1*, 225−238.
(23) Han, D.; Liu, X.; Wu, S. Metal Organic Framework-based Antibacterial Agents and Their Underlying Mechanisms. *Chem. Soc. Rev.* **2022**, *51*, 7138−7169.
(24) Alhidary, I. A.; Abdelrahman, M. M. Effects of Naringin Supplementation on Productive Performance, Antioxidant Status and Immune Response in Heat-Stressed Lambs. *Small Ruminant Res.* **2016**, *138*, 31−36.
(25) Hidalgo, T.; Simon-Vazquez, R.; Gonzalez-Fernandez, A.; Horcajada, P. Cracking the Immune Fingerprint of Metal-Organic Frameworks. *Chem. Sci.* **2022**, *13*, 934−944.
(26) Sugiura, M.; Ohshima, M.; Ogawa, K.; Yano, M. Chronic Administration of Satsuma Mandarin Fruit (*Citrus unshiu* MARC.) Improves Oxidative Stress in Streptozotocin-Induced Diabetic Rat Liver. *Biol. Pharm. Bull.* **2006**, *29*, 588−591.
(27) Horcajada, P.; Serre, C.; Vallet-Regi, M.; Sebban, M.; Taulelle, F.; Ferey, G. Metal-Organic Frameworks as Efficient Materials for Drug Delivery. *Angew. Chem., Int. Ed.* **2006**, *45*, 5974−5978.
(28) Dong, Z.; Sun, Y.; Chu, J.; Zhang, X.; Deng, H. Multivariate Metal−Organic Frameworks for Dialing-in the Binding and Programming the Release of Drug Molecules. *J. Am. Chem. Soc.* **2017**, *139*, 14209−14216.
(29) Karimi Alavijeh, R.; Akhbari, K. Biocompatible MIL-101(Fe) as a Smart Carrier with High Loading Potential and Sustained Release of Curcumin. *Inorg. Chem.* **2020**, *59*, 3570−3578.
(30) Almáši, M.; Zeleňák, V.; Palotai, P.; Beňová, E.; Zeleňáková, A. Metal-Organic Framework MIL-101(Fe)-NH_2 Functionalized with Different Long-Chain Polyamines as Drug Delivery System. *Inorg. Chem. Commun.* **2018**, *93*, 115−120.
(31) Ebadi, A.; Rafati, A. A. Development of Novel Biodegradable Enrofloxacin−Silica Composite for In Vitro Drug Release Kinetic Studies. *J. Polym. Environ.* **2018**, *26*, 3404−3411.
(32) Ganji, F.; Vasheghani Farahani, S.; Vasheghani-Farahani, E. Theoretical Description of Hydrogel Swelling: A Review. *Iran. Polym. J.* **2010**, *19*, 375−398.
(33) Rezaei-Sadabady, R.; Zarghami, N.; Barzegar, A.; Eidi, A.; Akbarzadeh, A.; Rezaei-Tavirani, M. Studies of the Relationship between Structure and Antioxidant Activity in Interesting Systems, Including Tyrosol, Hydroxytyrosol Derivatives Indicated by Quantum Chemical Calculations. *Soft* **2013**, *02*, 13−18.
(34) Han, L.; Fu, Q.; Deng, C.; Luo, L.; Xiang, T.; Zhao, H. Immunomodulatory Potential of Flavonoids for the Treatment of Autoimmune Diseases and Tumour. *Scand. J. Immunol.* **2021**, *95*, No. e13106.
(35) Balakrishnan, B.; Dooley, J. F.; Kopia, G.; Edelman, E. R. Intravascular Drug Release Kinetics Dictate Arterial Drug Deposition, Retention, and Distribution. *J. Controlled Release* **2007**, *123*, 100−108.